Supplement of Biogeosciences, 22, 641–657, 2025
https://doi.org/10.5194/bg-22-641-2025-supplement

Biogeosciences Open Access EGU

Supplement of

The effect of carbonate mineral additions on biogeochemical conditions in surface sediments and benthic–pelagic exchange fluxes

Kadir Biçe et al.

Correspondence to: Kadir Biçe (bicekadir@gmail.com) and Christof Meile (cmeile@uga.edu)

Supplementary Materials

Experimental setup

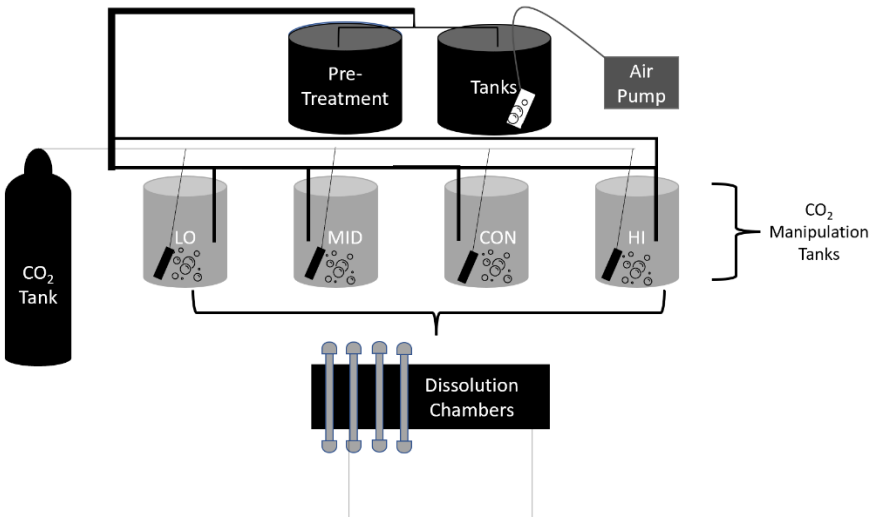

Figure S1: Simplified schematic of the flow through feedback-controlled seawater system used for the mineral dissolution experiments. The pre-treatment tanks contained seawater filtered to 5 microns from Yaquina Bay and were vigorously bubbled with ambient air. Water was pumped from the pre-treatment tanks to the CO_2 manipulation tanks (Lo, Mid, Con, Hi) and excess water was then circulated back. CO_2 treatment tanks were manipulated using lab-grade CO_2 to generate specific $\Omega_{calcite}$ in a feedback-controlled system measuring $pH_{(NBS)}$. The pH in each CO_2 manipulation tank was monitored using an Apex-Controller manipulation system (Neptune Systems Energy Bar 832 interfaced with an Apex Controller Base Unit and pH/ORP probe modules: PM1). One double junction pH probe was located in the recirculation return line in each CO_2 manipulation tank. All pH probes were calibrated at the beginning of each experiment using pH 4, 7, and 10 NBS buffers, to obtain a three-point calibration curve.

Table S1: Table of measured TCO_2, pCO_2, Temperature (T), Salinity (S), measured pH_{NBS} and subsequently calculated saturation state ($\Omega_{calcite}$) from seawater tank discrete (pCO_2/TCO_2) samples associated with our flow through feedback-controlled seawater system. For each dissolution trial, a total of four pCO_2/TCO_2 samples were used. Measurements following procedures from Bandstra et al. (2006), modified for discrete samples as in Hales et al. (2005), Barton et al., (2012), and Hales et al. (2017). The temperature (^oC) listed is from in situ measurements recorded from within the water treatment tanks (does not reflect experimental temperatures)

TCO_2 (µmol/kg)	pCO_2 (µatm)	T (^oC)	Salinity	Measured pH_{NBS}	Calculated $\Omega_{calcite}$
2530.7	8589.3	18	33.1	6.85	0.25
2340.1	4569.2	18	33.2	7.14	0.45
2291.5	2537.9	19	33.4	7.28	0.85
2252.8	1946.2	18	33.2	7.46	1.03

The correlation between measured benchtop pH data and the pH data from the experimental system for header tanks in all experiments was consistently an R^2 greater than 0.9 across all experiments (Figure S2).

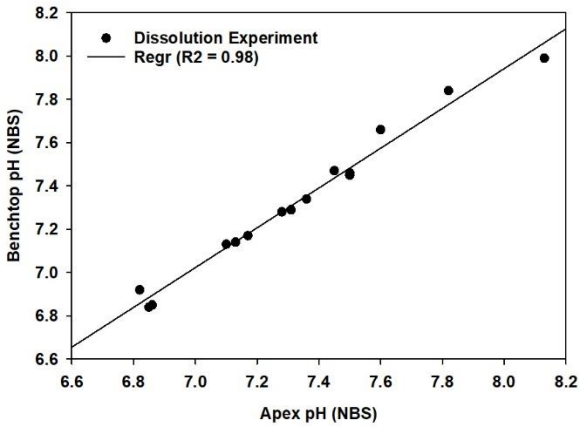

Figure S2: Measured pH_{NBS} from a benchtop probe and the pH_{NBS} from the experimental system in the flowthrough feed-back controlled seawater system tanks

Effect of the dilution due to mineral addition

We carried out addition simulations in which we assumed that the addition of minerals at the top replaces OM, lowering the OM concentration in the top 2 cm. To estimate the potential impact of dilution due to replacing OM with PIC, we simulated OM as state variable and using a rate expression $R_C = k*OM$, replacing the imposed OM reaction rates $R_C = R_C^0 *\exp(-x/\gamma_{om})$. We assumed that the proportion of addition of PIC is the same as removal of the OM (i.e., adding 8% of mineral means lowering OM concentration by 8%). The rate constant k was set to 0.25 yr^{-1}, chosen to approximate the rates computed in the $R_C(z)$ approach. Flux of carbon was taken from literature as ~510 µmol cm^{-2} yr^{-1} (Thullner et al., 2009).

Figure S3 shows before and after the addition of minerals when dilution is present. We compared these results against a simulation with dilution turned off. The impact of dilution was minimal with slight reductions observed mainly in OM mineralization processes which resulted in decreases in TA production rates. Production of TA production was reduced by 17 and 33 µmol cm^{-2} yr^{-1} for 8% and 16% applications respectively.

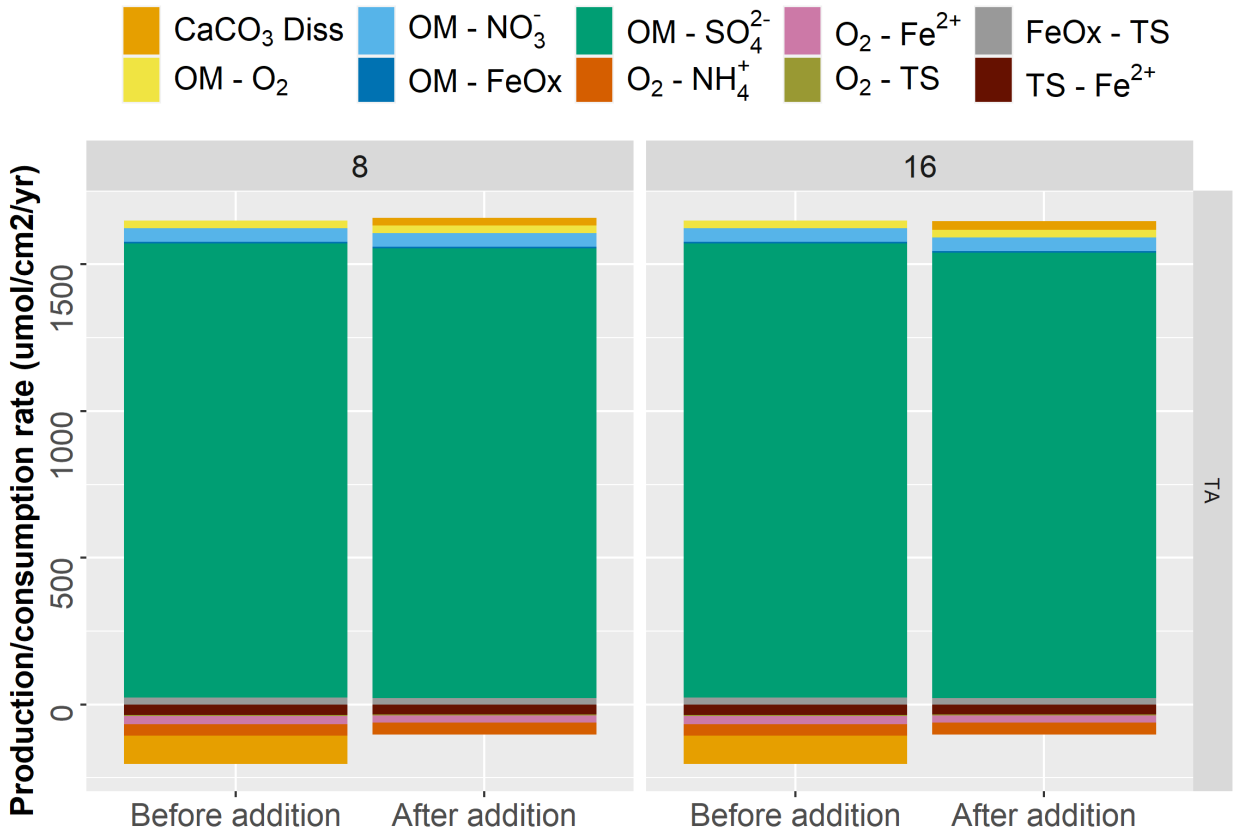

Figure S3. Production of TA for different amounts of mineral added when dilution is considered (8 = 8% mineral addition, 16 = 16% mineral addition).

The buffering factor (dpH/dTA)

We also computed dpH/dTA as the buffering factor (Figure S4). We observed decreasing values of dpH/dTA with time in all scenarios. This illustrates that as buffering develops and TA levels are higher, a further increase in TA has a reduced impact on pH. Deeper mixed layer (high ML) showed larger values which are due to elevated mixing of minerals leading to increases in the impact of dissolution-based TA production on pH. After 2 years, the low R_C^0 scenario produced slightly negative dpH/dTA which hinted to the suppression of mineral dissolution due to less acidification (i.e., although smaller, TA production is done by OM mineralization which also decreases pH).

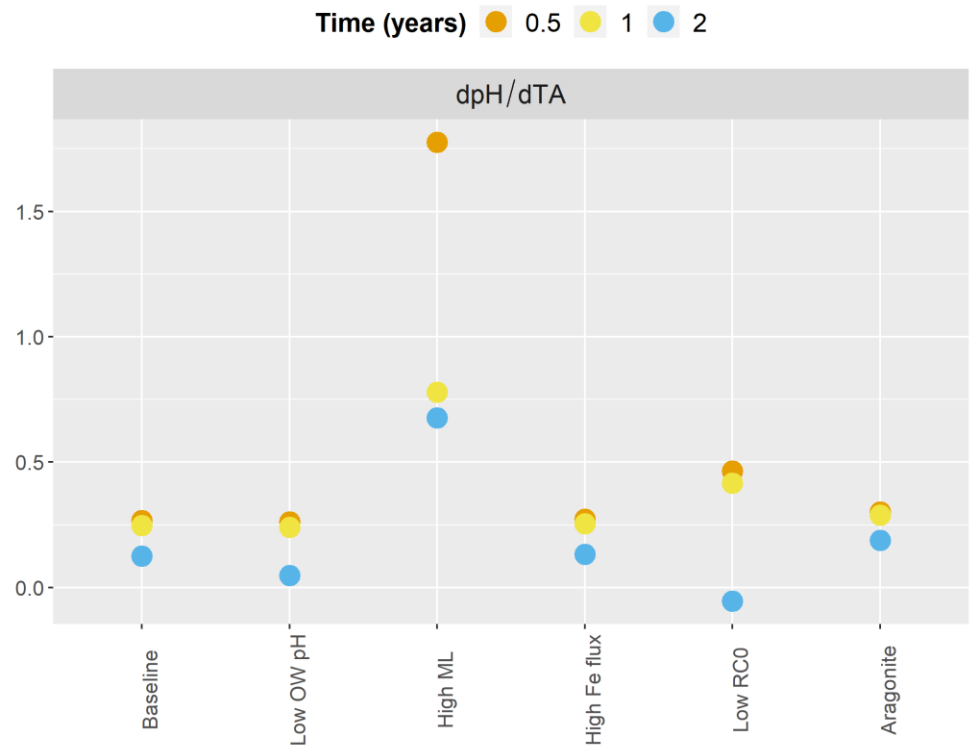

Figure S4: dpH/dTA for different scenarios at the top 10cm of the sediment

Box model for atmospheric DIC uptake

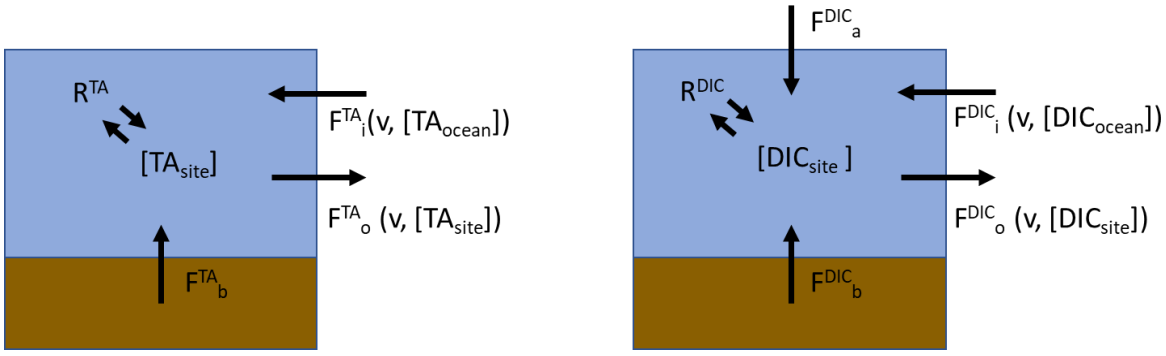

Figure S5: Schematic of water column TA and DIC fluxes for Yaquina Bay.

The water exchange rate was approximated from measurements of water height. Using a 3 m semidiurnal tidal range from NOAA South Beach, OR (Station ID: 9435380) station, a representative exchange velocity is $2.1*10^5$ cm/yr .

For pre-addition scenario, benthic TA and DIC fluxes were taken from the model as 1100 and 1121 µmol cm^{-2} yr^{-1} respectively. TA mass balance equation was solved for R^{TA} using $[TA_{ocean}]$ as 2.2 and $[TA_{site}]$ as 1.9 mmol L^{-1} (measured at Hatfield Marine Station). Then, R^{DIC} was estimated using R^{TA} with respiration producing NO_3^-/primary production consuming NO_3^-

(coupled respiration and nitrification). $[DIC_{site}]$ and $[DIC_{ocean}]$ were calculated using site and ocean TA and pH using aquaenv R package as 1.8 and 2.1 µmol cm^{-3} respectively. Lastly, F_a^{DIC} was estimated by DIC mass balance.

After the addition of minerals, benthic fluxes were 1227 and 1185 µmol cm^{-2} yr^{-1} for TA and DIC. $[TA_{site}]$ and $[DIC_{site}]$ were recalculated using mass balance with R^{TA} and R^{DIC}. pH of the site was assumed to be constant from pre-addition and the resulting changes in $[TA_{site}]$ and $[DIC_{site}]$ were in the order of 10^{-3} µmol/cm^3. This assumption was in line with Hickey & Banas (2003) who state that the estuarine water column biogeochemical processes are driven by oceanic source water and process, given the large tidal prism and relatively small volume in this and other Pacific Northwest estuaries.

The flux of CO_2 between the atmosphere and the water showed that the bay is net heterotrophic with emission fluxes of 458352 and 458294 µmol cm^{-2} yr^{-1} before and after the addition, respectively. Impact of buffering on F_a^{DIC} was calculated as additional 58 µmol cm^{-2} yr^{-1} CO_2 flux into the water column during the peak buffering period which is trivial compared to the tidal CO_2 exchange fluxes. However, scaling these estimates up would produce considerable changes compared to anthropogenic C in US Pacific coastal waters (Pacella et al., 2024).

We explored the sensitivity of air-sea CO_2 fluxes to the pH in the bay, as well as the magnitude of the tidal exchange between the bay and the coastal ocean. CO_2 uptake due to mineral addition was slightly sensitive to pH in the bay (a change of approximately 1.4 µmol cm^{-2} yr^{-1} per change in 0.1 pH unit in range 7.86-7.96). However, since the CO_2 uptake due to mineral additions were calculated as the difference between two scenarios, altering the tidal input (tidal exchange volume, dTA, dDIC) did not have a considerable impact on the impact of buffering (not shown).

References:

Bandstra, L., Hales, B., & Takahashi, T. (2006). High-frequency measurements of total CO2: Method development and first oceanographic observations. Marine Chemistry, 100(1-2), 24-38.

Barton, A., Hales, B., Waldbusser, G. G., Langdon, C., & Feely, R. A. (2012). The Pacific oyster, Crassostrea gigas, shows negative correlation to naturally elevated carbon dioxide levels: Implications for near-term ocean acidification effects. Limnology and oceanography, 57(3), 698-710.

Hales, B., Takahashi, T., & Bandstra, L. (2005). Atmospheric CO2 uptake by a coastal upwelling system. Global Biogeochemical Cycles, 19(1).

Hales, B., Suhrbier, A., Waldbusser, G. G., Feely, R. A., & Newton, J. A. (2017). The carbonate chemistry of the "fattening line," Willapa Bay, 2011–2014. Estuaries and Coasts, 40, 173-186.

Hickey, B. M., & Banas, N. S. (2003). Oceanography of the US Pacific Northwest coastal ocean and estuaries with application to coastal ecology. *Estuaries*, *26*, 1010-1031.

Pacella, S. R., Brown, C. A., Labiosa, R. G., Hales, B., Mochon Collura, T. C., Evans, W., & Waldbusser, G. G. (2024). Feedbacks between estuarine metabolism and anthropogenic CO2

accelerate local rates of ocean acidification and hasten threshold exceedances. Journal of Geophysical Research: Oceans, 129(3), e2023JC020313.

Thullner, M., Dale, A. W., & Regnier, P. (2009). Global-scale quantification of mineralization pathways in marine sediments: A reaction-transport modeling approach. Geochemistry, geophysics, geosystems, 10(10).